

## Manuscript Details

<b>Manuscript number</b>	IJRMHM_2019_865_R1
<b>Title</b>	Effect of milling conditions and binder phase content on liquid phase sintering of heat treatable WC-Ni-Co-Cr-Al-Ti cemented carbides
<b>Article type</b>	Research Paper

### Abstract

The binder phase of WC based cemented carbides has been alloyed by adding two different aluminium compounds, AlN and TiAl<sub>3</sub>, to mixtures comprised of WC, Ni, Co and Cr<sub>3</sub>C<sub>2</sub> powders. A more efficient alloying effect is obtained by TiAl<sub>3</sub> additions likely due to its higher dissolution rate during liquid phase sintering. Shrinkage and melting phenomena are strongly affected by the energy of the milling process and the amount of metallic additions. The use of higher milling rotation speed induces higher oxidation of the powder mixtures and the subsequent formation of a higher volume fraction of alumina particles after sintering. Densification and WC grain growth are hindered by increasing the Al addition. Thus, full densification of alloys with higher Al additions require the use of HIP after standard vacuum sintering cycles. As-HIPed WC-Ni-Co-Cr-Al-Ti samples present a binder phase with precipitation of gamma prime similar to that found in as-cast Ni superalloys. The size, volume fraction and morphology of these precipitates has been modified by applying a standard solution treatment (1150°C-2 h) followed by fast air cooling and subsequent aging at 600°C and different dwelling times. Age hardening effects have been confirmed in the composition consisting of WC-12wt.% Co-12wt.% Ni-1.7wt.% Cr<sub>3</sub>C<sub>2</sub>-5wt.% TiAl<sub>3</sub> after 100 hours at this temperature.

<b>Keywords</b>	WC hardmetals, Al alloying, sintering, HIP, gamma prime precipitation
<b>Corresponding Author</b>	Jose M. Sanchez
<b>Corresponding Author's Institution</b>	CEIT-IK4
<b>Order of Authors</b>	Tomas Soria Biurrun, Belen Lopez Ezquerra, Lorena Lozada, Jose M. Sanchez

## Submission Files Included in this PDF

### File Name [File Type]

Cover letter.doc [Cover Letter]

answer to referee comments.docx [Response to Reviewers]

HIGHLIGHTS.docx [Highlights]

Manuscript\_revised.doc [Manuscript File]

Fig. 1.ppt [Figure]

Fig. 2.ppt [Figure]

Fig. 3.ppt [Figure]

Fig. 4.ppt [Figure]

Fig. 5.ppt [Figure]

Fig. 6.ppt [Figure]

Fig. 7.ppt [Figure]

Fig. 8.ppt [Figure]

Fig. 9.ppt [Figure]

Fig. 10.ppt [Figure]

Table 1.docx [Table]

Table 2.docx [Table]

Table 3.docx [Table]

Table 4.docx [Table]

conflict of interests.docx [Conflict of Interest]

CRedit author statement.docx [Author Statement]

To view all the submission files, including those not included in the PDF, click on the manuscript title on your EVISE Homepage, then click 'Download zip file'.

## Research Data Related to this Submission

There are no linked research data sets for this submission. The following reason is given:  
Data will be made available on request

Nov. 21<sup>st</sup>, 2019

Dear Editor:

We would like to submit the article entitled “Effect of milling conditions and binder phase content on liquid phase sintering of heat treatable WC-Ni-Co-Cr-Al-Ti cemented carbides” for publication in the International Journal of Refractory Metals and Hard Materials. Please, do not hesitate to contact us if you have any questions.

Yours sincerely,



J.M. Sánchez

CEIT-IK4 . Paseo Manuel de Lardizabal, 15, 20018, San Sebastián, Spain.

phone: 34-943-212800  
fax:34-943-213076  
email: [jmsanchez@ceit.es](mailto:jmsanchez@ceit.es)

**Ref: IJRMHM\_2019\_865**

**Title: Effect of milling conditions and binder phase content on liquid phase sintering of heat treatable WC-Ni-Co-Cr-Al-Ti cemented carbides**

**Journal: International Journal of Refractory Metals and Hard Materials**

Thank you very much for your comments and reviewing work. Sorry for these mistakes.

Editor and Reviewer Comments:

### **Reviewer 1**

- Some English grammar issues should be revised and modified:

\* 2nd line of 2nd paragraph of Introduction: "harDmetals" **DONE**

\* Within 1st paragraph of Section 3(a) - "... WC mean grain ... for Alloy 1 THAN (?) in Alloy 2 ..." (please modified sentence). **The modified sentence is as follows: " WC mean grain sizes are higher for alloy 1 than for alloy 2 (2.1  $\mu\text{m}$  vs. 1.2  $\mu\text{m}$  respectively)**

\* Within 2nd paragraph of Section 3(b) - "... are close between 2 and 3 ..." (please modified sentence). **The new sentence is as follows: "The largest alumina particles found in this alloy are found after milling at 100 rpm and their sizes range between 2 and 3  $\mu\text{m}$ ".**

\* Within 1st paragraph of Section 3(c) - "That is, ... Alloy 3." (English grammar could be improved here) **This sentence has been removed and substituted by this one: "Thus,  $\gamma$  precipitates found in Alloy 4 are smaller than those corresponding to Alloy 2 and the same happens for Alloys 5 and 3".**

\* Within 6th paragraph of Section 3(c) - "... the same metallic content but lower aluminium ..." (please modified sentence) **DONE**

\* Within 6th paragraph of Section 3(c) - use "with" instead of "to" after "associated" (twice at the end of the referred paragraph) **DONE**

\* Within Figure 4's caption: "... at 100 rpm, (d) Alloy 3 at 100 rpm...." **We have included the word "milled" in all cases between the alloy reference and the milling condition.**

- Other issues:

\* Please define within the contribution the meaning of FSSS as well as D50. **DONE. FSSS stands for Fisher sub-sieve size and D50 is the particle size at 50% on the cumulative frequency of the log-normal distribution.**

\* Figure 2 and Table 2 are not referred within the text (?). **Sorry, we forgot to do it. Figure 2 is cited now in Line 15 in section 3. Results and discussion. Table 2 was cited in line 21 of the same section and also in section 3b in line 24**

\* Please include "accessed date" within ref 1 **DONE. Jan-7<sup>th</sup>-2020**

\* Ref 7 is missing additional coauthors **DONE.**

\* Ref 19 is missing "title" of the publication **DONE.**

## HIGHLIGHTS

### **Effect of milling conditions and binder phase content on liquid phase sintering of heat treatable WC-Ni-Co-Cr-Al-Ti cemented carbides.**

- 1- Heat treatable WC based cemented carbides have been obtained by liquid phase sintering of WC-Ni-Co-Cr<sub>3</sub>C<sub>2</sub> powder mixtures including Al containing powders. Best alloying effect is obtained with TiAl<sub>3</sub> additions.
- 2- Densification and WC grain growth are hindered by increasing the Al addition for a constant metallic content.
- 3- Full densification with high Al contents requires the use of HIP after conventional vacuum sintering.
- 4- Al-rich oxides are produced during the milling process. The volume fraction of these oxides increases with the milling rotation speed.
- 5- As-HIPed WC-Ni-Co-Cr-Al-Ti samples present a binder phase with precipitation of gamma prime similar to that found in as-cast Ni superalloys.
- 6- The size, volume fraction and morphology of these precipitates has been modified by applying a standard solution treatment (1150°C-2 h) followed by fast air cooling and subsequent aging at 600°C and different dwelling times.

## **Effect of milling conditions and binder phase content on liquid phase sintering of heat treatable WC-Ni-Co-Cr-Al-Ti cemented carbides**

Tomas Soria Biurrun<sup>1,2</sup> [tsoria@ceit.es](mailto:tsoria@ceit.es); Belen Lopez Ezquerro<sup>1,2</sup> [belen\\_1988@hotmail.com](mailto:belen_1988@hotmail.com); Lorena Lozada Cabezas<sup>1,2</sup> [llozada@ceit.es](mailto:llozada@ceit.es) ; Jose M. Sánchez Moreno<sup>1,2</sup> [jmsanchez@ceit.es](mailto:jmsanchez@ceit.es)

1- CEIT-IK4, Manuel Lardizabal 15, 20018 Donostia / San Sebastián, Spain.

2- UNIVERSIDAD DE NAVARRA, Tecnun, Manuel Lardizabal 13, 20018 Donostia / San Sebastián, Spain.

### **Abstract**

The binder phase of WC based cemented carbides has been alloyed by adding two different aluminium compounds, AlN and TiAl<sub>3</sub>, to mixtures comprised of WC, Ni, Co and Cr<sub>3</sub>C<sub>2</sub> powders. A more efficient alloying effect is obtained by TiAl<sub>3</sub> additions likely due to its higher dissolution rate during liquid phase sintering. Shrinkage and melting phenomena are strongly affected by the energy of the milling process and the amount of metallic additions. The use of higher milling rotation speed induces higher oxidation of the powder mixtures and the subsequent formation of a higher volume fraction of alumina particles after sintering. Densification and WC grain growth are hindered by increasing the Al addition. Thus, full densification of alloys with higher Al additions require the use of HIP after standard vacuum sintering cycles. As-HIPed WC-Ni-Co-Cr-Al-Ti samples present a binder phase with precipitation of gamma prime similar to that found in as-cast Ni superalloys. The size, volume fraction and morphology of these precipitates has been modified by applying a standard solution treatment (1150°C-2 h) followed by fast air cooling and subsequent aging at 600°C and different dwelling times. Age hardening effects have been confirmed in the composition consisting of WC-12wt.% Co-12wt.% Ni-1.7wt.% Cr<sub>3</sub>C<sub>2</sub>-5wt.% TiAl<sub>3</sub> after 100 hours at this temperature.

### **1. Introduction**

The expansion of the electric vehicle market will increase exponentially the demand for cobalt in the next decade [1,2]. Therefore, finding alternative materials for cobalt replacement in WC-Co alloys is now a priority of the hardmetal industry. High entropy alloys (HEA) and other multicomponent metallic binders have been recently identified as possible candidates for this purpose [3-7]. In the case of WC-HEA alloys, fully dense materials have been obtained by liquid phase sintering (LPS) of near-equiatomic

compositions including at least 4 of these elements: Co, Cr, Cu, Fe and/or Ni. Moreover, it has to be taken into account that, in all cases, a certain amount of W is dissolved in the binder phase during sintering depending on the C activity [7]. In these alloys, it is assumed that all these metallic elements form a single austenitic binder phase stabilized by its configurational entropy. However, it is still unclear if precipitation of deleterious secondary phases is completely avoided, specially as Cr content increases [8].

Apart from Fe-Ni-Co-Cr materials, some metallic or intermetallic alloys containing aluminium, like Ni-Al or Fe-Al, have also been investigated for cobalt replacement in hardmetals, mainly for their potential gamma prime precipitation hardening effect [7,9-12]. However, due to their complexity, very little is known yet about their microstructural characteristics, processing issues and final physico-chemical properties. In a previous work [6], it has been shown that non-isoatomic combinations of Co, Ni, Cr, Ti and Al can be used to obtain heat treatable WC-Co-Ni-Cr-Al-Ti materials with precipitation of  $\gamma'$ -type phases. This work is focused on analyzing this  $\gamma'$  precipitation under different aging conditions. Moreover, two key aspects of powder processing of these materials will be also discussed: the effect of milling conditions and the use of different Al containing powders as precursors for Al alloying during sintering.

## 2. Experimental procedure

Composition of the powder mixtures are included in Table 1. A WC powder with a mean particle size of 3.7  $\mu\text{m}$  and a constant Co/Ni ratio of 50/50 in wt.% was used in all cases. Fisher sub-sieve sizes (FSSS) of Co and Ni powders were 2.2 and 1.2 microns respectively. Two types of compositions were prepared with two different Co+Ni contents: 24 wt.% (Alloys 1, 2 and 3) and 12 wt.% (Alloys 4 and 5). Chromium was added via  $\text{Cr}_3\text{C}_2$  carbide powders (FSSS =1.5 microns). The total Cr content was calculated to keep a constant Cr/(Co+Ni) ratio of 0.06 in all compositions. According to previous works, this avoids the precipitation of Cr-rich  $\text{M}_7\text{C}_3$  carbides [13,14]. Two different Al compounds were selected for alloying the binder phase: titanium aluminide ( $\text{TiAl}_3$ ) and aluminium nitride (AlN) powders (FSSS values equal to 35 and 28 microns respectively). Although both powders are coarser than the rest of materials used in the mixtures, they are brittle enough to ensure its homogeneous distribution in the powder mixtures during milling. The melting point of  $\text{TiAl}_3$  is  $\approx 1350^\circ\text{C}$ , a temperature slightly higher than the melting range measured by DSC for W-C-Co-Ni-Cr alloys (between  $1205^\circ\text{C}$  and  $1284^\circ\text{C}$  depending on their C content [14]). However, it is below the sintering temperatures required for full densification of these materials (between  $1400$  and  $1475^\circ\text{C}$ )[14]. The melting point of aluminium

nitride (AlN) is much higher ( $>2500^{\circ}\text{C}$ )[15]. However, it has been selected because, in previous works, it was claimed that avoids the formation of oxides during heating [11]. Taking this into account, two different Al/(Co+Ni) wt.% ratios were investigated: 0.08 for Alloys 1, 2 and 4 and 0.13 for Alloys 3 and 5. Mixing/milling was carried out in a planetary equipment for 5 hours using hexane as liquid media and a ball to powder wt. ratio of 6. Two different rotation speeds were used: 100 and 200 rpm. Paraffin, used as pressing aid, was added in the last milling hour. Afterwards, the powders were dried for 1 h at atmospheric pressure in a thermostatic bath ( $90\pm 2^{\circ}\text{C}$ ). Green compacts were obtained by double action pressing at 160 MPa. The sinterability of the different powder mixtures was analysed by calorimetry, thermogravimetry (TGA/DSC Setaram Setsys Evolution 16/18) and dilatometry (Netzsch TA 402 E/7). These experiments were carried out on 5 mm high and 5 mm  $\phi$  cylinders using a heating rate of  $10^{\circ}\text{C}/\text{min}$  up to  $1450^{\circ}\text{C}$ . Dwelling time at this temperature was 1 hour for dilatometric experiments and 5 min. for DSC/TGA tests (both types of experiments were made in Ar atmosphere, 1 bar). The onset of DSC and shrinkage rate peaks were determined by using the SETSOFT software [16]. Sintering experiments were carried out in a industrial vacuum furnace with graphite heating elements at a heating rate of  $10^{\circ}\text{C}/\text{min}$  up to  $1300^{\circ}\text{C}$ . The vacuum level used during this step was  $10^{-2}$  mbar. Above this temperature, pressure was increased up to 100 mbar by injecting argon in the furnace chamber and maintained during the rest of the sintering cycle. Under such conditions, the temperature was raised up to  $1400^{\circ}\text{C}$  and maintained during 1 h. The whole process will be referred to as "VS" in the rest of the text. Standard ISO 3369 was used for measuring the density of VS specimens. From these data, it was decided to apply a hot isostatic pressing treatment (HIP) in order to eliminate any residual porosity. These cycles were carried out at  $1400^{\circ}\text{C}$  and 150 MPa for 1 hour. Before applying aging treatments, all VS+HIP specimens were solution treated in Ar at  $1150^{\circ}\text{C}$  for 2 h followed by rapid air cooling. Aging experiments were carried only in compositions milled at 100 rpm due to their lower oxide contents. These tests were performed at  $600^{\circ}\text{C}$  and three different dwelling times: 1, 10 and 100 h. Finally, the sintered specimens were ground and polished down to 1  $\mu\text{m}$  diamond paste for microstructural analysis, which was carried out by optical and scanning electron microscopy (FEG-SEM) and energy dispersive X-ray spectroscopy (EDS). Phase identification was carried out by X-Ray diffraction (XRD) (with Ni-filtered  $\text{CuK}\alpha$  radiation) using Bragg-Brentano configuration. Vickers hardness of aged specimens was measured by using 10 kg. of applied load (ISO 3878).



### 3. Results and discussion

#### (a) Selection of additives for Al alloying of the binder phase in WC-Co-Ni-Cr cemented carbides

Alloys 1 and 2 were designed to study the dissolution of AlN and TiAl<sub>3</sub> compounds in the binder phase of WC-Co-Ni-Cr materials. Both compositions were processed under low energy milling conditions (i.e. 100 rpm). Fully dense specimens were obtained after pressing and sintering as described in the previous section (Fig. 1). EDS analyses corresponding to Alloy 1 confirm that the grains in black contrast pointed by red arrows in Fig. 1a are AlN grains which are not dissolved in the binder phase after sintering. In Alloy 2, there are also dark precipitates (Fig. 1b), but, in this case, EDS analyses prove that are Al-rich oxides and no TiAl<sub>3</sub> particles. As previously described [6], these aluminium rich oxides are likely formed by direct reaction between TiAl<sub>3</sub> and the different oxides present in the powder mixtures (i.e. those of Co, Ni, W or even Cr) in competition with the carbothermal reduction typically described for WC-Co materials[17]. Although a precise analysis of the Al content of the binder phase in these materials requires TEM samples, EDS-SEM data already show that the amount of aluminium dissolved in the binder phase of Alloy 2 (with TiAl<sub>3</sub> additions) is higher than that found in Alloy 1 (with AlN additions) (Fig. 2). This suggests that, although some aluminium is lost to the reduction of powder oxides in Alloy 2, there is still more aluminium available for alloying the Co-Ni-Cr metallic binder phase than in Alloy 1 (with AlN additions). These different dissolution rates of AlN and TiAl<sub>3</sub> particles in the liquid phase generated during sintering of WC-Co-Ni-Cr materials indicate that, as expected from their melting points, the chemical stability of TiAl<sub>3</sub> is lower than that of AlN. WC mean grain sizes measured by mean linear intercept method are higher for Alloy 1 than for Alloy 2 (2.1 μm vs. 1.2 μm respectively) (Fig. 1 and Table 2). This result is consistent with previous findings that prove the role of aluminium as an efficient WC grain growth inhibitor during sintering [6]. Thus, a finer microstructure is obtained when more Al is dissolved in the binder phase during sintering WC-Co-Ni-Cr alloys. This effect is also reflected in the shape of WC grains: more faceted in the case of AlN additions and more rounded for the material with TiAl<sub>3</sub>. This result indicates that when a certain amount of aluminium is dissolved in the liquid phase, the preferential growth of (0001) basal planes in WC crystals is modified by altering likely both the WC dissolution process and the two-dimensional nucleation-controlled coarsening process [18-20].

Another difference between materials processed with AlN or TiAl<sub>3</sub> additions is that, after the decomposition of the latter, titanium is released in the system. Similarly to that observed in P-grades,

titanium is combined with W and C precipitating (Ti,W)C cubic carbides, which are identified by their light grey contrast in BSE-SEM images (marked by green arrows in Fig. 1b).

Taking into account these results, it was decided to focus on materials with  $\text{TiAl}_3$  additions due to their higher solubility in the binder phase of WC-Co-Ni-Cr materials.

(b) Densification of WC-Co-Ni-Cr<sub>3</sub>C<sub>2</sub>-TiAl<sub>3</sub> compositions

Dilatometric experiments show that the densification of WC-Co-Ni-Cr<sub>3</sub>C<sub>2</sub>-TiAl<sub>3</sub> alloys is more sensitive to milling conditions than to the  $\text{TiAl}_3$  content. Alloy 2 and 3 exhibit similar shrinkage curves when milled at 100 rpm and both increase their total shrinkage when milled at 200 rpm (solid and dotted curves in Fig. 3a respectively). Shrinkage rates during the heating ramp are, in both cases, approx. one order of magnitude higher for the specimens milled at 200 rpm (Fig. 3b). The correlation between shrinkage and melting phenomena is summarised in Table 3. The temperatures corresponding to maximum shrinkage rates are compared with those of DSC endothermic peaks linked to liquid formation (Fig. 3c). As expected from their high metallic content, shrinkage always precedes melting in all cases. These results agree with those reported for WC-Co materials in which solid state sintering mechanisms are enhanced by increasing the milling energy (i.e. increasing the powder surface area) [21]. Under such conditions, there is also a higher plastic deformation of the metallic particles, which also enhances atomic diffusion. It is also worth noting that the areas over the DSC endothermic peaks of both Alloys 2 and 3 are slightly reduced when using higher milling energy. This suggests that the amount of liquid during sintering is lower than in the case of powders milled at 100 rpm.

Microstructural characterization was carried out to analyze this phenomenon. BSE-SEM images of Alloys 2 and 3 after densification by VS+HIP show the dramatic reduction of WC grain size produced by increasing the milling rotation speed (Fig. 4). It has to be remembered that WC starting powder powders have a mean particle size equal to  $3.7\mu\text{m}$ . This value corresponds to 50% on the cumulative frequency of the log-normal distribution. The fraction of WC grains with sizes below  $1\mu\text{m}$  is significantly higher for Alloy 3 (with a nominal Al content 66% higher than Alloy 2). This agrees with previous results in which the role of Al as WC grain growth inhibitor during LPS was already proven [6]. Oxygen contents of sintered specimens obtained by IR spectrometry, included in Fig. 4, confirm that powder oxidation increases significantly by increasing the milling energy (120% for Alloy 2 and 56% for Alloy 3) (Table 2). As the milling energy increases, the particle size of all constituents in the powder mixtures decrease, specially that of  $\text{TiAl}_3$  particles. Therefore, a higher surface area is

exposed to ambient conditions leading to higher powder oxidation, specially of those containing aluminium. For Alloy 2, the volume fraction of Al-rich oxides (which appear embedded in the metallic binder phase) is below 0.02 % when milled at 100 rpm and rises to 0.6 vol.% after milling at 200 rpm. The mean grain size of these Al-rich oxides ranges from 0.1 to 0.5  $\mu\text{m}$ . For Alloy 3, both the mean size and volume fraction of alumina precipitates increase. The largest alumina particles found in this alloy are found after milling at 100 rpm and their sizes range between 2 and 3  $\mu\text{m}$ . Summarizing, both the sinterability and the microstructure of WC-Co-Ni-Cr<sub>3</sub>C<sub>2</sub>-TiAl<sub>3</sub> are significantly modified by the milling process. Powders are strongly oxidized when milled at 200 rpm, thus increasing the final volume fraction of Al-rich oxides retained in the microstructure after sintering. It is worth noting that as more aluminium is lost to the formation of Al-rich oxides, less Al is available to alloy the metallic binder. This finding agrees with the lower amount of liquid detected after high energy milling of Alloys 2 and 3 (Fig. 3c).

The effect of the amount of Co+Ni addition on shrinkage has been investigated in materials milled at 100 rpm. As expected from any LPS system with good wetting behaviour, shrinkage increases with the amount of Co+Ni, that is, with the amount of liquid phase. This is confirmed both in dilatometric and calorimetric experiments (Fig. 5). Thus, Alloys 2 and 3 (both with Co+Ni = 24 wt.%) have 46% more shrinkage than Alloys 4 and 5 (both with Co+Ni= 12 wt.%) (Fig. 5a). DSC data show that melting starts at temperatures 40-45°C higher for the alloys with higher aluminium content, independently of their Co+Ni content. In addition, areas above DSC peaks are 50-60% lower for the Alloys with lower Co+Ni content (i.e. Alloys 4 and 5), which corroborates the lower amount of liquid phase in these materials. Shrinkage rates are also strongly modified by Co+Ni additions. Thus, Alloys 2 and 3 exhibit only one peak and Alloys 4 and 5 show two peaks separated by 60°C-80°C respectively (Fig. 5c). This suggests that solid and liquid phase sintering mechanisms overlap in alloys with 24 wt.% Co+Ni metallic addition. In solid state, the plastically deformed metallic powders tend to spread on the surface of WC grains causing densification by rearrangement. This process is likely enhanced by the presence of crystalline defects in the FCC lattice (induced by milling), but its driving force decreases as the powder is annealed during the heating ramp. At the same time, creep due to dislocation climbing and vacancy diffusion increases until the formation of the liquid phase.

In Alloys 4 and 5 (with half Co+Ni content), shrinkage slows down between 1280-1300°C and 1338-1340°C. This phenomenon could be due to the fact that solid state sintering mechanisms are less

active in this temperature range and that the amount of liquid phase is still too low for maintaining the shrinkage rate. This is not observed in Alloys 2 and 3 because the amount of liquid phase is higher.

Although shrinkage is limited in compositions with low binder phase content (Alloys 4 and 5), full density specimens have been obtained by applying the sintering procedure described in the experimental setup (Fig. 6). As previously described for high binder phase materials, these images show that as Al content increases, WC grain sizes decrease. This confirms that aluminium dissolution in the binder phase inhibits WC grain growth during sintering. On the other hand, the volume fraction of Al-rich oxides also increases with the aluminium content.

### (c) Gamma prime precipitation in WC-Co-Ni-Cr<sub>3</sub>C<sub>2</sub>-TiAl<sub>3</sub> materials

One of the most interesting properties of WC-Co-Ni-Cr<sub>3</sub>C<sub>2</sub>-TiAl<sub>3</sub> materials is the precipitation of  $\gamma'$  phases in their metallic binders in a duplex structure similar to that found in as-cast Ni superalloys. These precipitates, easily distinguished by their darker contrast in comparison with the Co-Ni-Cr-W based matrix, are already present in as-HIPed specimens (Fig. 7). As observed in these images,  $\gamma'$  precipitates are smaller for Alloys 2 and 4 (those with lower nominal Al content). It is also worth noting that  $\gamma'$  mean sizes are smaller and their particle size distributions are narrower for the compositions with lower amount of metallic phase, independently of their nominal aluminium content. Thus,  $\gamma'$  precipitates found in Alloy 4 are smaller than those corresponding to Alloy 2 and the same happens for Alloys 5 and 3. Although the reason is still unclear, it could be related to the higher thermal conductivity of cemented carbides as their tungsten carbide content increases [22]. Taking this into account, it is possible that Alloys 4 and 5 are cooled at a higher rate than Alloys 2 and 3, which would promote homogeneous over heterogeneous  $\gamma'$  nucleation.

No differences in contrast within the binder phase are observed in solution treated specimens for all compositions (Fig. 8). However, this changes completely in the samples aged at 600°C for 100 hours (compare Figs. 7, 8 and 9). In Alloy 2, the most intense peak of binder phase after solution treatment is  $\gamma$  (200) (Fig. 10a). This changes gradually with the aging time at 600°C. Thus, after 1 hour at 600°C,  $\gamma'$  (111) peak is already stronger than that of  $\gamma$  (200). This trend continues for longer times until  $\gamma$  (200) disappears after 100 h. at 600°C. Peaks of  $\gamma$  and  $\gamma'$  phases are not separated in this material suggesting that differences in their lattice parameters are below the resolution limit of this technique.

Anyhow, SEM images obtained from Alloy 2 aged specimens show no clear evidences of  $\gamma'$  precipitation (Fig. 9a).

In the case of Alloy 3 (with the same Co+Ni content as Alloy 2 but higher Al addition), the most intense XRD peak after solution treatment is  $\gamma$  (111). After 1 hour at 600°C, this peak is shifted towards  $\gamma'$  (111). For longer dwelling times, both peaks are present in the specimens. Therefore, as the Al content increases,  $\gamma$  and  $\gamma'$  phases are easier to distinguish by XRD. In this case, SEM images show clear differences in contrast within the binder phase which agree with XRD results (Figs. 9b and 10b). However, the morphology of  $\gamma$  and  $\gamma'$  phases is very different from the cuboids observed after HIPing (see Fig. 7).

In compositions with lower (Co+Ni) content (Alloys 4 and 5), the XRD peaks of the binder phase have lower intensities than in Alloys 2 and 3 (Fig. 10). Moreover, the peaks corresponding to solution treated samples are more shifted towards those of  $\gamma'$ -Ni<sub>3</sub>Al phase (ICDD ref. pattern 03-065-6613). A certain separation between peaks of  $\gamma$  and  $\gamma'$  phases is observed in Alloy 4, suggesting that the solution treatment is not as efficient as in the compositions with higher Co+Ni contents. As aging time increases, XRD shifting towards lower diffraction angles continues which is consistent with additional  $\gamma'$  precipitation (as observed in Fig. 9c).

Finally, in Alloy 5 (with half Co+Ni content of Alloy 2 and higher Al/(Co+Ni) ratio), diffraction peaks corresponding to the binder phase are similar in solution treated and aged specimens. Even in solution treated specimens, XRD peaks of the binder phase are already close to those of  $\gamma'$  phase. Although some differences in contrast can be observed in the corresponding BSE-SEM images (Fig. 9d),  $\gamma'$  precipitates are not easily identified in this material. TEM investigations are being carried out for a more detailed analysis of these extremely fine phases.

The effect of the different thermal treatments on the overall hardness of WC-Co-Ni-Cr<sub>3</sub>C<sub>2</sub>-TiAl<sub>3</sub> materials is shown in Table 4. These data confirm that age hardening effects at 600°C are only observed in the composition with higher aluminium and binder phase contents (Alloy 3). In Alloy 2 (with the same metallic content but lower aluminium content), precipitation hardening is very small (i.e. within resolution error bands). In Alloys 4 and 5, with lower metallic content, the hardness of the composite is controlled by the hardness of the WC phase and its contiguity [23]. Therefore, any age hardening effect associated with the metallic binder is below the scattering associated with the

hardness of the WC phase. Nanoindentation and hot hardness experiments are being carried out in order to characterize these phenomena.

#### **4. Conclusions**

Heat treatable WC-Co-Ni-Cr-Ti-Al cemented carbides have been obtained in fully dense form by HIP after sintering. Al alloying of the binder phase is better achieved by using  $TiAl_3$  additions in the powder mixtures. As expected, the sinterability of these new compositions decreases by reducing the amount of (Co+Ni) metallic additions and by increasing their Al content. Powder milling has a significant effect in these materials since Al oxides induced during this process cannot be reduced by carbothermal reactions.  $\gamma'$  precipitation within the binder phase of these cemented carbides is already observed in as-HIP specimens, that is under very low cooling rates. On the other hand, these compositions are susceptible to solution reprecipitation treatments like those used in as-cast Ni superalloys. Aging treatments carried out at 600°C and different dwelling times show that the volume fraction, size and morphology of  $\gamma'$  phases is very different from those obtained after HIPing. Vickers hardness tests confirm age hardening effects in the alloy with higher (Co+Ni) and Al contents. In alloys with lower amount of metallic additions, the overall hardness of these ceramic-metal composites is dominated by the volume fraction and contiguity of WC grains. Therefore, age hardening effects induced in the metallic binder are below the resolution of macroscopic hardness experiments.

#### **Acknowledgments**

CDTI (Centro para el Desarrollo Tecnológico Industrial) and the Department of Education of the Navarra Government are gratefully acknowledged by the financial support of this work.

#### **References**

- 1- <https://mmta.co.uk/2017/09/20/consequences-for-cobalt/>. Accessed date; Jan-7<sup>th</sup>-2020
- 2- P. Alves, D. Blagoeva, C. Pavel, N. Arvanitidis, Cobalt: demand-supply balances in the transition to electric mobility, JRC Science for policy report, <https://ec.europa.eu/jrc/en>. European Commission, 2018.

- 3- C.-S. Chen, C.-C. Yang, H.-Y. Chai, J.-W. Yeh, J.L.H. Chau, Novel cermet material of WC/multi-element alloy, *Int. J. Refract. Met. Hard Mater.* 43 (2014) 200–204.
- 4- L. Toller, C.X. Liu, E. Holmström, T. Larsson, S. Norgren, Investigation of cemented carbides with alternative binders after CVD coating, *Int. J. Refract. Met. Hard Mater.* 62 (2017) 225–229.
- 5- D. Linder, E. Holmström, S. Norgren, High entropy alloy binders in gradient sintered hardmetal, *Int. J. Refract. Met. Hard Mater.* 71 (2018) 217–220
- 6- B. Lopez Ezquerro, T. Soria Biurrun, L. Lozada Cabezas, J M.Sánchez Moreno, F. Ibarreta Lopez, R. Martinez Pampliega, Sintering of WC hardmetals with Ni-Co-Cr-Ti-Al multi-component alloys, *Int. J. Refract. Met. Hard Mater.*, 77, 2018: 44-53
- 7- J. García, V. Collado Ciprés, A. Blomqvist, B. Kaplan, Cemented carbide microstructures: a review, *Int. J. Refract. Met. Hard Mater.*, 80 (2019) 40-68.
- 8- R. de Oro, C. Edtmaier, W.-D. Schubert, Novel binder phases for WC-based cemented carbides with high Cr contents, *Int. J. Refract. Met. Hard Mater.*, 85 (2019) 105063.
- 9- J. Long, Z. Zhang, T. Xu, B. Lu, Microstructure, mechanical properties and fracture behavior of WC-40 vol.% Ni<sub>3</sub>Al composites with various carbon contents, *Int. J. Refract. Met. Hard Mater.* 40 (2013) 2–7
- 10- J. Long, W. Zhang, Y. Wang, Y. Du, Z. Zhang, B. Lu, K. Cheng, Y. Peng, A new type of WC–Co–Ni–Al cemented carbide: Grain size and morphology of  $\gamma'$ -strengthened composite binder phase *Scripta Mater.*, 126 (2017), 33-36.
- 11- K. Nishigaki, H. Doi, N. Yukawa, M. Morinaga, T. Koie, Binder phase strengthening through  $\gamma'$  precipitation of WC-Co-Ni-Cr-Al hard alloys, HM30, *Proc. of 11th Plansee Seminar* (1985) 487-508.
- 12- R.K.Viswanadham, P.G.Lindquist and J.A.Peck: *Science of Hard Materials*, *Proc. of 1st International Conference on Science of Hard Materials*, Eds. R.K.Viswanadham, D.J. Rowcliffe, J. Gurland, Plenum Press, (1983), 873-889.
- 13- I. Iparraguirre, N. Rodriguez, F. Ibarreta, R. Martinez and J.M. Sanchez, Effect of the Cr content on the sintering behaviour of TiCN-WC-Ni-Cr<sub>3</sub>C<sub>2</sub> powder mixtures, *Int. J. Refract. Met. Hard Mater.* 43 (2014) 125–131.

- 14- M. Aristizabal, J.M. Sanchez, N. Rodriguez, F. Ibarreta and R. Martinez. "Liquid phase sintering and oxidation resistance of WC-Ni-Co-Cr cemented carbides" *Int. J. Refract. Met. Hard Mater.* 28 (2010) 516-522.
- 15- W.M. Haynes, *CRC Handbook of Chemistry and Physics* (97th ed.). CRC Press. ed. (2016). p. 4.45.
- 16- SETARAM Instrumentation. *Setsys evolution 16/18. SETSOFT user manual*, (2002), 39.
- 17- C.H. Allibert, Sintering features of cemented carbides WC-Co processed from fine powders, *Int. J. Refract. Met. Hard Mater.* 19 (2001) 53-61.
- 18- H. Fischmeister, G. Grimval In: Kuczynski GC, editor. *Sintering and Related Phenomena*. New York: Plenum Press; (1980) 119–149.
- 19- H.E. Exner, Fischmeister H., Structure of sintered tungsted carbide-cobalt alloys, *Arch fd Eisenhuttenwesen*, (1966); 37(2): 417–426.
- 20- Y.J. Park, N.M. Hwang, D.Y. Yoon, Abnormal growth of faceted (WC) grains in a (Co) liquid matrix, *Metall. Mater. Trans. A*, 27A, (1996) 2809-2819.
- 21- G. Gille, B. Szesny, K. Dreyer, H. van den Berg, J. Schmidt, T. Gestrich, G. Leitner, Submicron and ultrafine grained hardmetals for microdrills and metal cutting inserts, HM1, 15<sup>th</sup>. *Int. Plansee Seminar*, Eds. G. Kneringer, P. Rödhammer, H. Wildner, Plansee Holding, AG, Reutte, (2001) Vol.2, 782-816.
- 22- H. Wang, T.Webb, J..W.Bitler, Study of thermal expansion and thermal conductivity of cementedWC–Co composite, *Int. J. Refract. Met. Hard Mater.* 49 (2015) 170-177.
- 23- J. Gurland, New scientific approaches to development of tool materials, *Int. Mat. Rev.* 33 (1988) 151-166.



## **Figure captions**

**Fig. 1** BSE-SEM images of VS+HIPed specimens:(a) Alloy 1 (2.86 wt.%AlN) (b) Alloy 2 (3.00wt.%TiAl<sub>3</sub>). EDS analyses correspond to the phases pointed by arrows of different colors: red for AlN particles, blue for Al-rich oxides and green for (Ti,W)C phases.

**Fig. 2** EDS analyses corresponding to the metallic binder phases of the materials shown in Fig. 1: (a) Alloy 1 (2.86 wt.%AlN) (b) Alloy 2 (3.00wt.%TiAl<sub>3</sub>). Additions correspond to the same amount of aluminium in both materials.

**Fig. 3** (a) Dilatometric curves corresponding to Alloys 2 and 3 processed at different milling rotation speeds, (b) Shrinkage rate curves corresponding to the same materials, (c) DSC curves showing the corresponding endothermic peaks obtained during the heating ramps of dilatometric experiments.

**Fig. 4** BSE-SEM images of Alloys 2 and 3 processed under different milling conditions: (a) Alloy 2 (3.00wt.%TiAl<sub>3</sub>) milled at 200 rpm, (b) Alloy 3 (5.00wt.%TiAl<sub>3</sub>) milled at 200 rpm, (c) Alloy 2 milled at 100 rpm, (d) Alloy 3 milled at 200 rpm. Oxygen contents measured by IR spectrometry for each material after VS+HIP are included at the lower right corner of the corresponding images.

**Fig. 5** (a) Dilatometric curves corresponding to Alloys 2, 3, 4 and 5 processed at 100 rpm, (b) Shrinkage rate curves corresponding to the same materials, (c) DSC curves showing the corresponding endothermic peaks obtained during the heating ramps of dilatometric experiments.

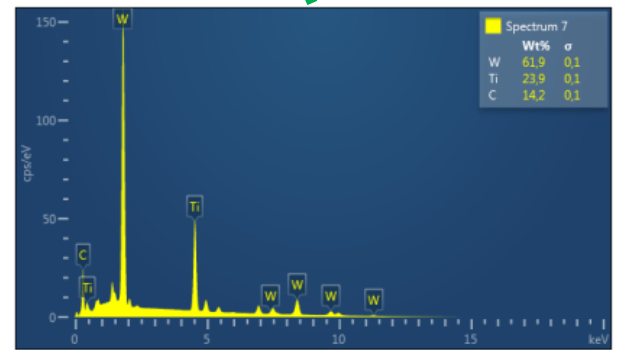
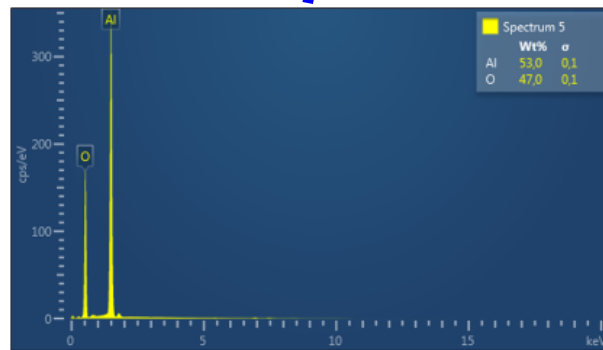
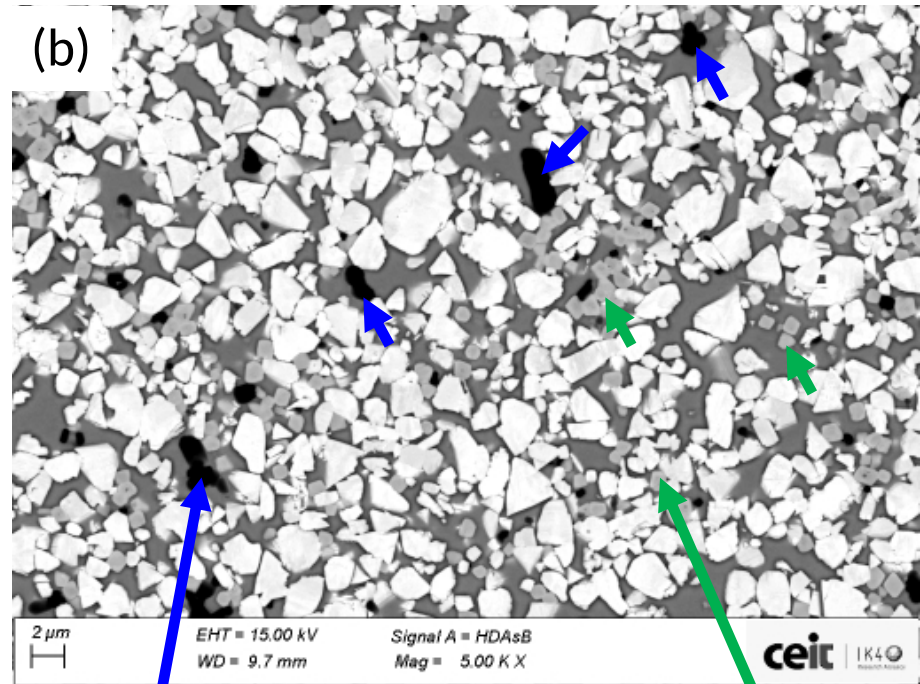
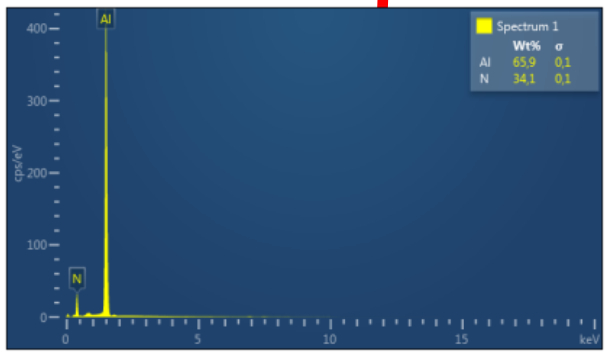
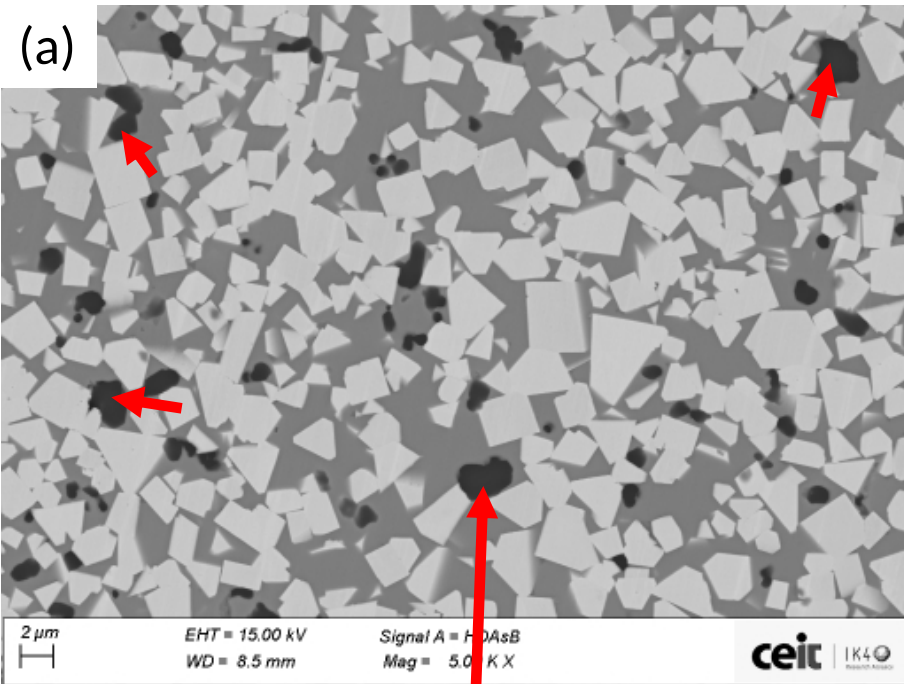
**Fig. 6.** BSE-SEM images corresponding to Alloys 4 and 5 (Co+Ni= 12wt.%): (a) Alloy 4, (b) Alloy 5. In both cases, Al-rich phases appear in dark contrast embedded in the metallic binder phase.

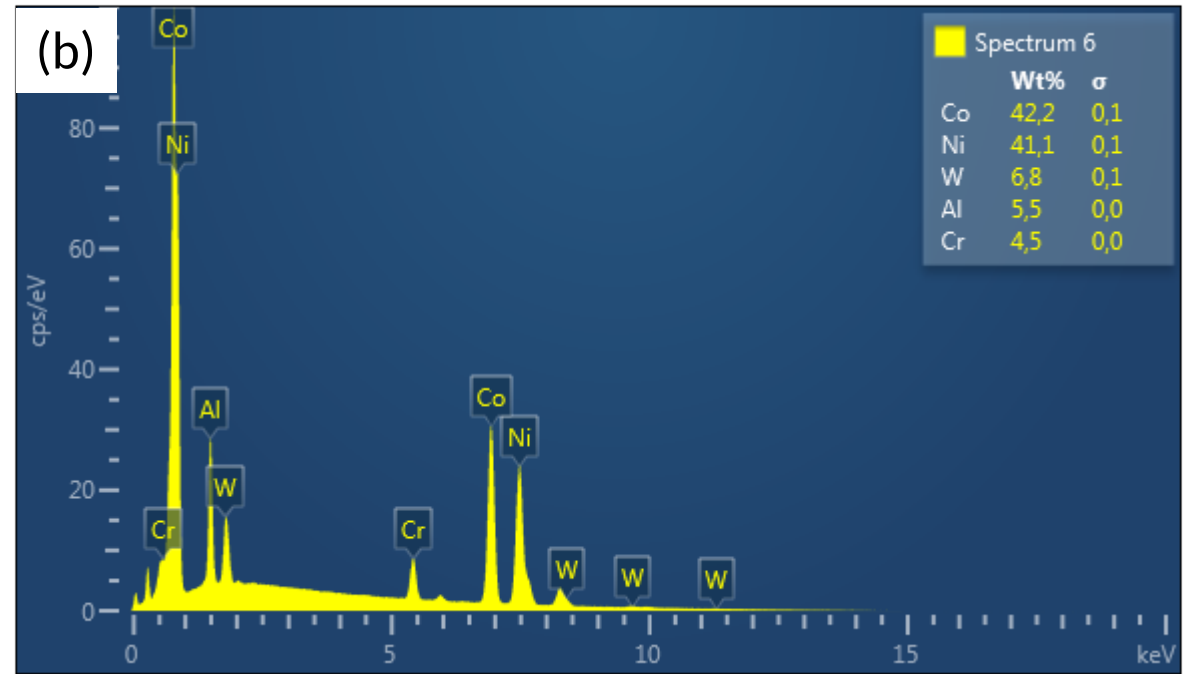
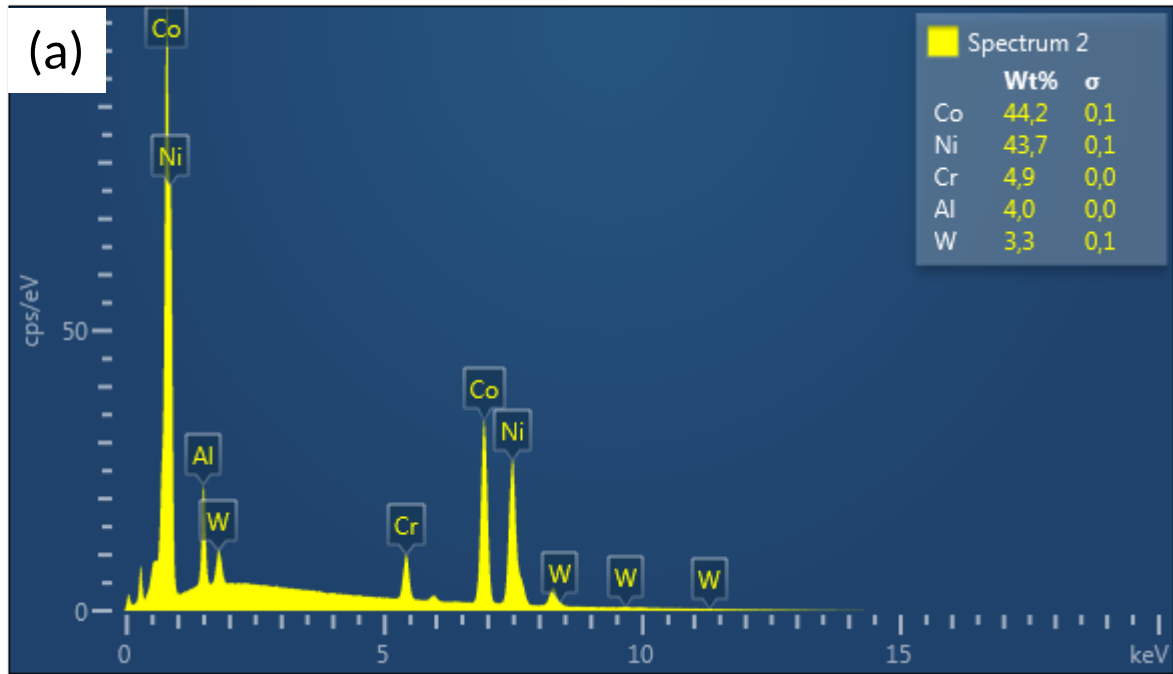
**Fig. 7** BSE-SEM images showing the microstructure of the metallic binder phase of WC-Co-Ni-Cr<sub>3</sub>C<sub>2</sub>-TiAl<sub>3</sub> alloys milled at 100 rpm after VS+HIP: (a) Alloy 2, (b) Alloy 3, (c) Alloy 4 and (d) Alloy 5.  $\gamma'$  precipitates appear in dark contrast embedded in the corresponding Co-Ni-Cr-Al-W binder phases.

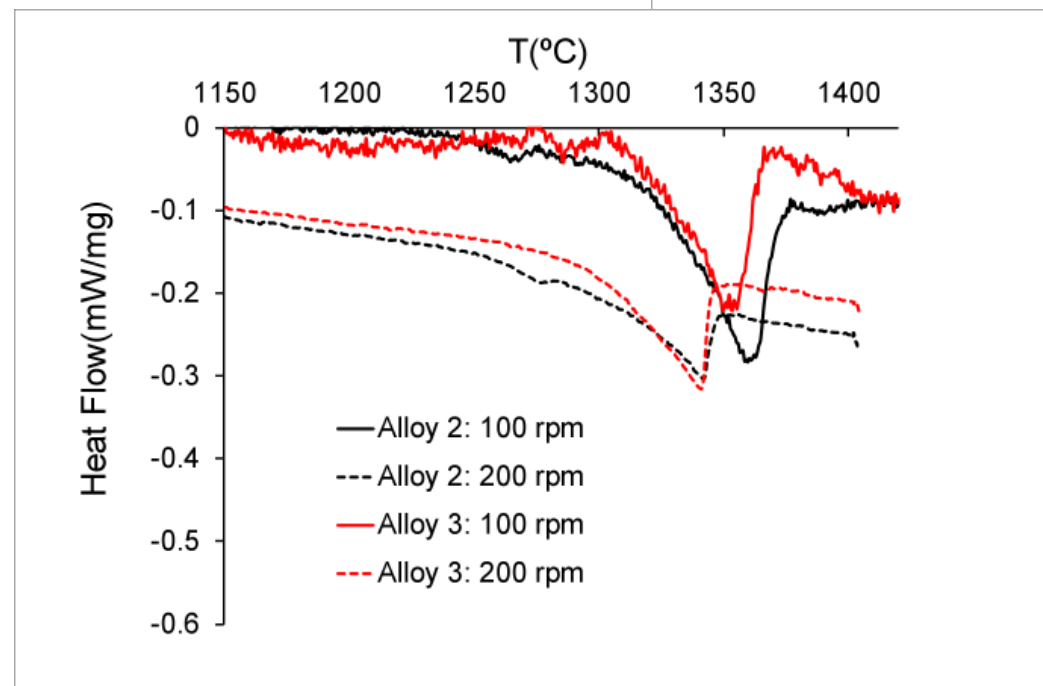
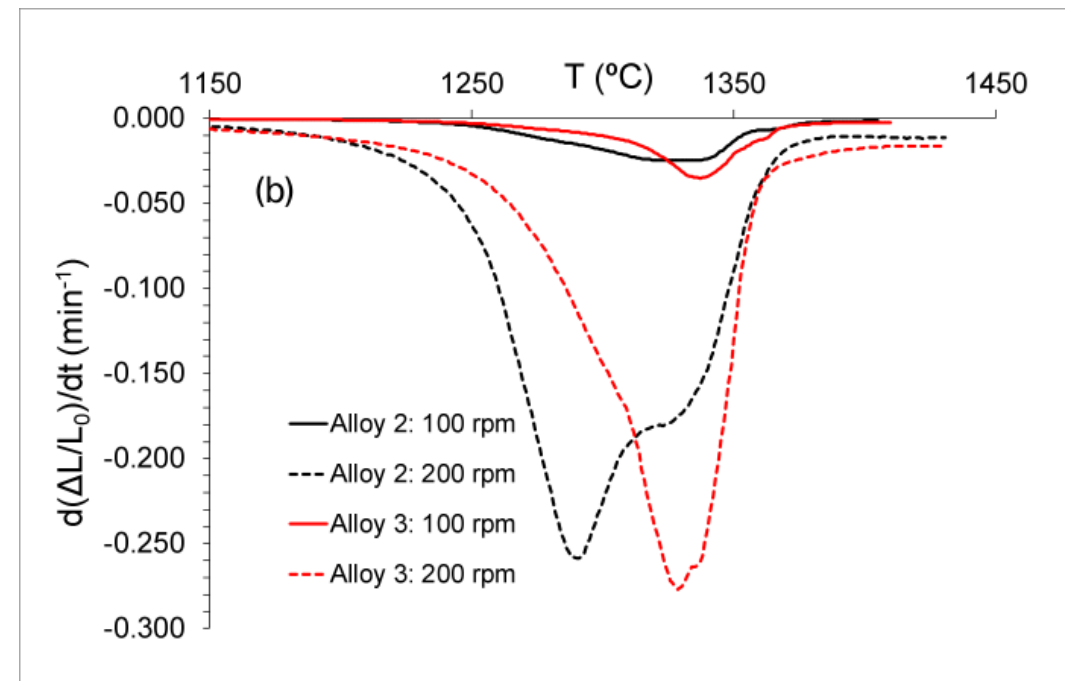
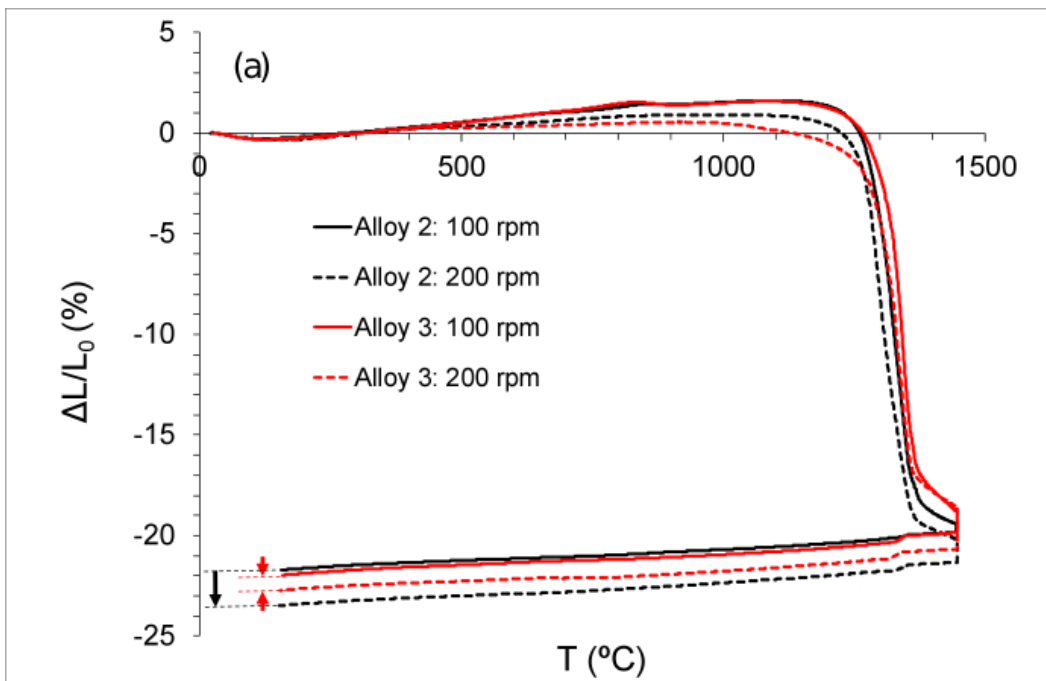
**Fig. 8** BSE-SEM images showing the microstructure of the metallic binder phase of WC-Co-Ni-Cr<sub>3</sub>C<sub>2</sub>-TiAl<sub>3</sub> alloys milled at 100 rpm after solution treatment at 1150°C for 2 hours: (a) Alloy 2, (b) Alloy 3, (c) Alloy 4 and (d) Alloy 5.

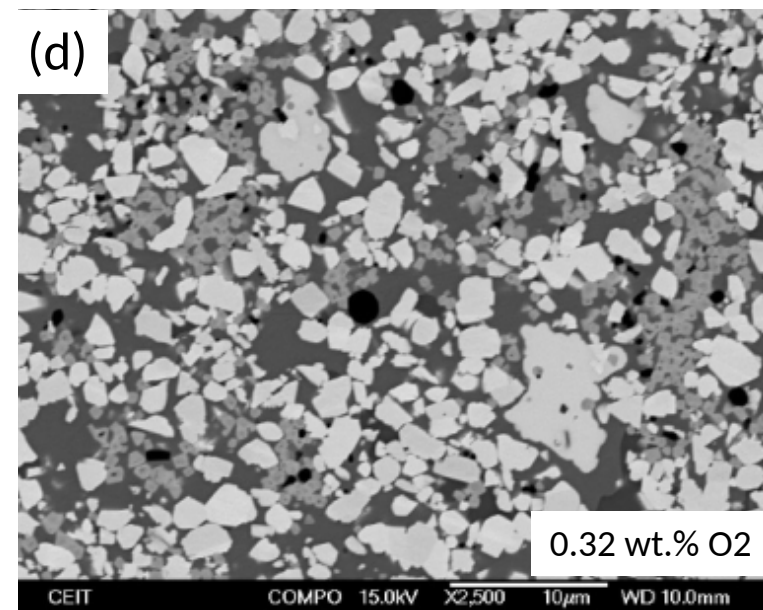
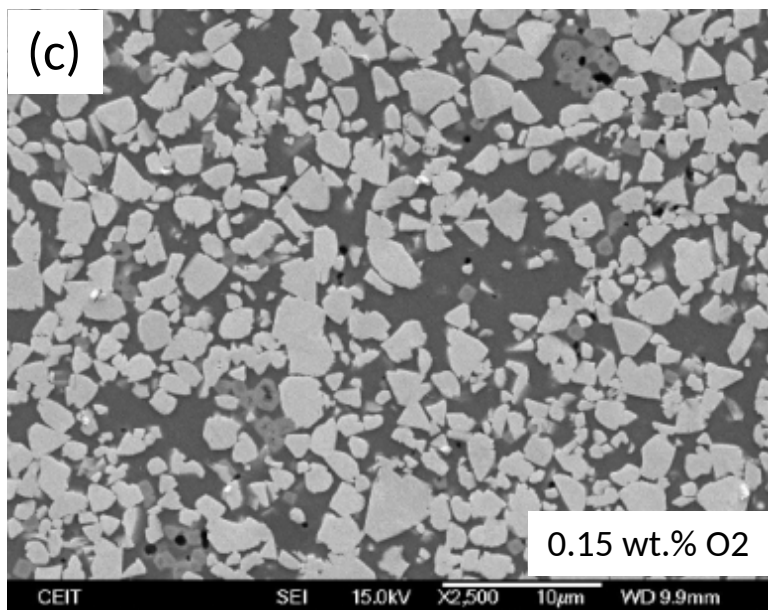
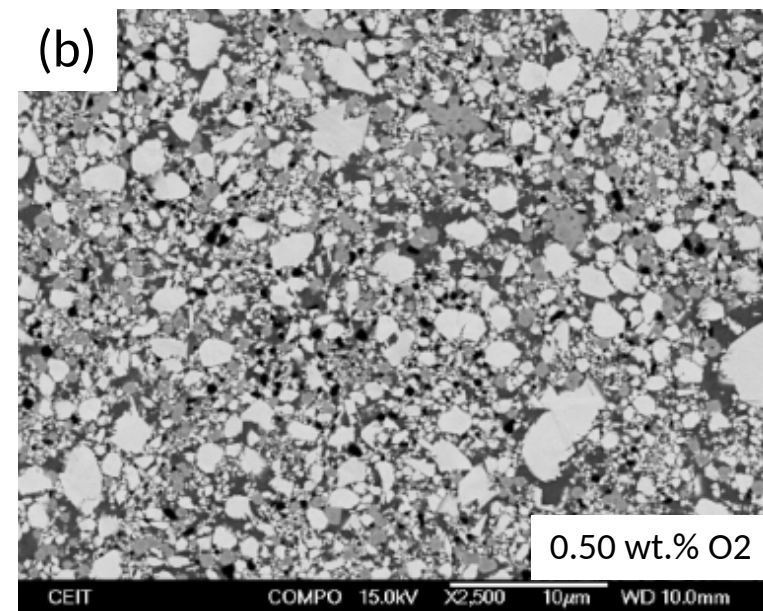
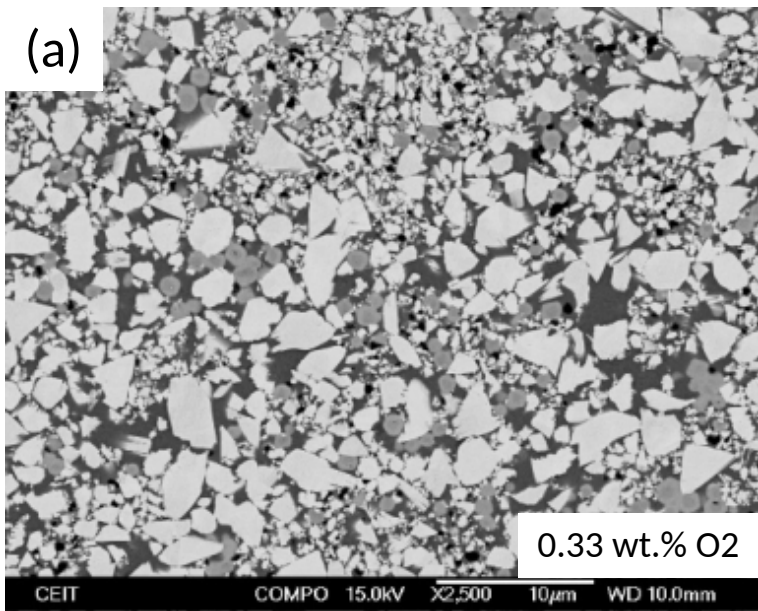
**Fig. 9** BSE-SEM images showing the microstructure of the metallic binder phase of WC-Co-Ni-Cr<sub>3</sub>C<sub>2</sub>-TiAl<sub>3</sub> alloys milled at 100 rpm after aging at 600°C for 100 hours: (a) Alloy 2, (b) Alloy 3, (c) Alloy 4 and (d) Alloy 5.

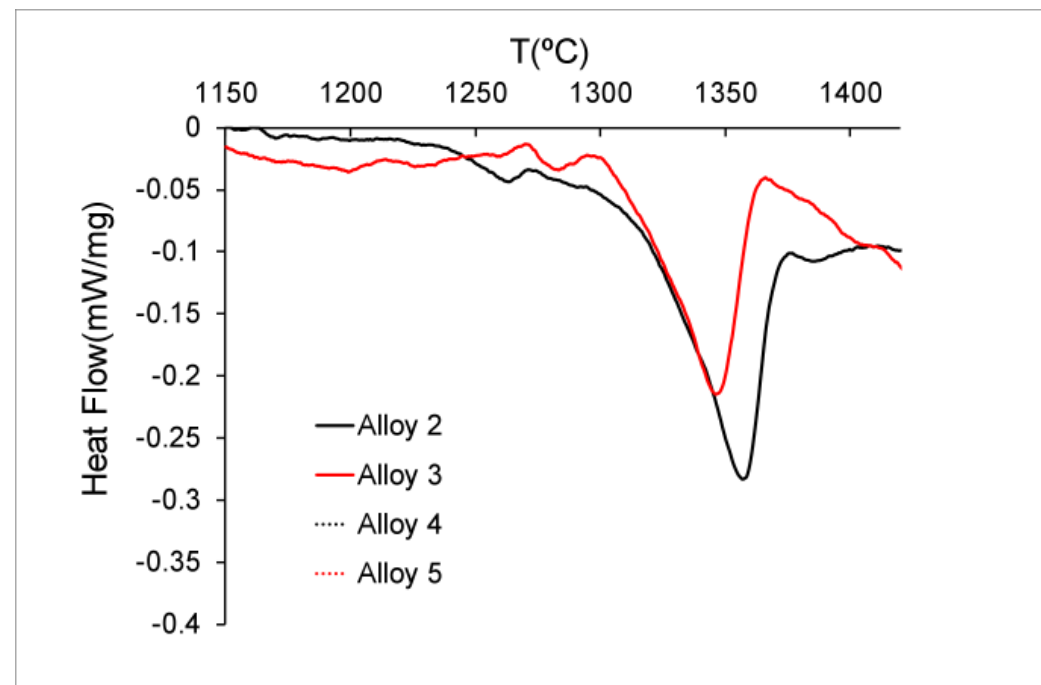
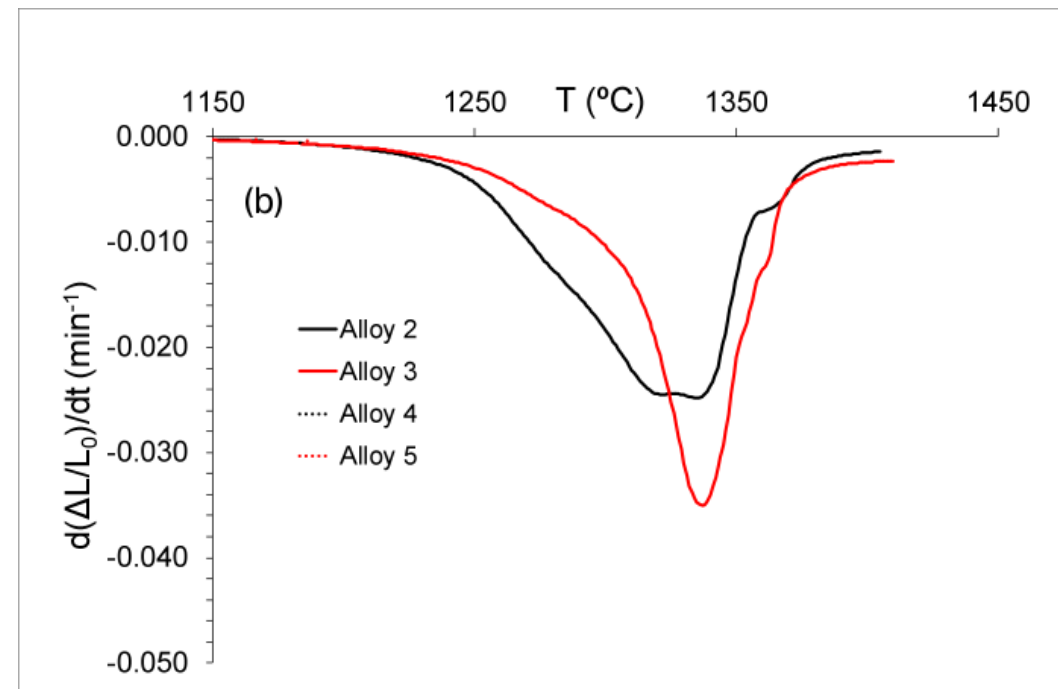
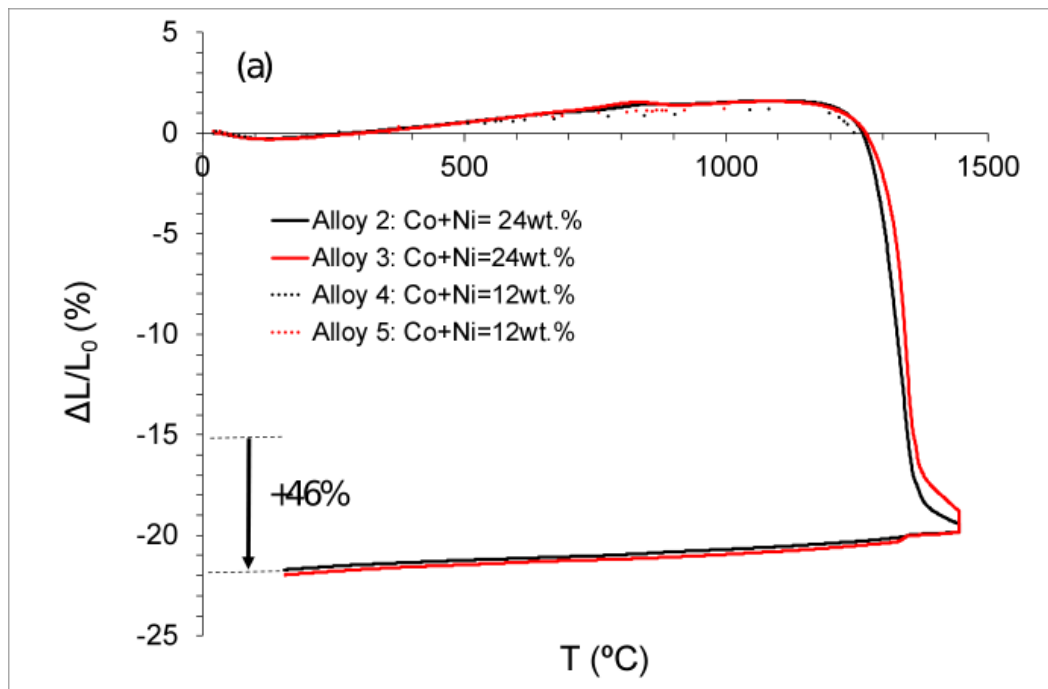
**Fig. 10** XRD patterns corresponding to WC-Co-Ni-Cr<sub>3</sub>C<sub>2</sub>-TiAl<sub>3</sub> alloys after different thermal treatments: (a) Alloy 2, (b) Alloy 3, (c) Alloy 4 and (d) Alloy 5.

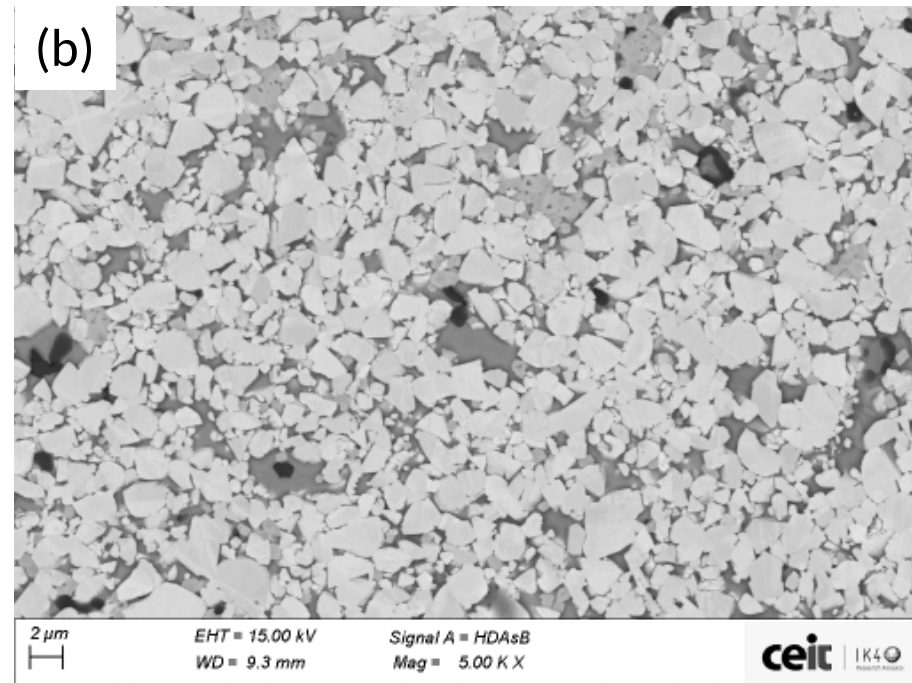
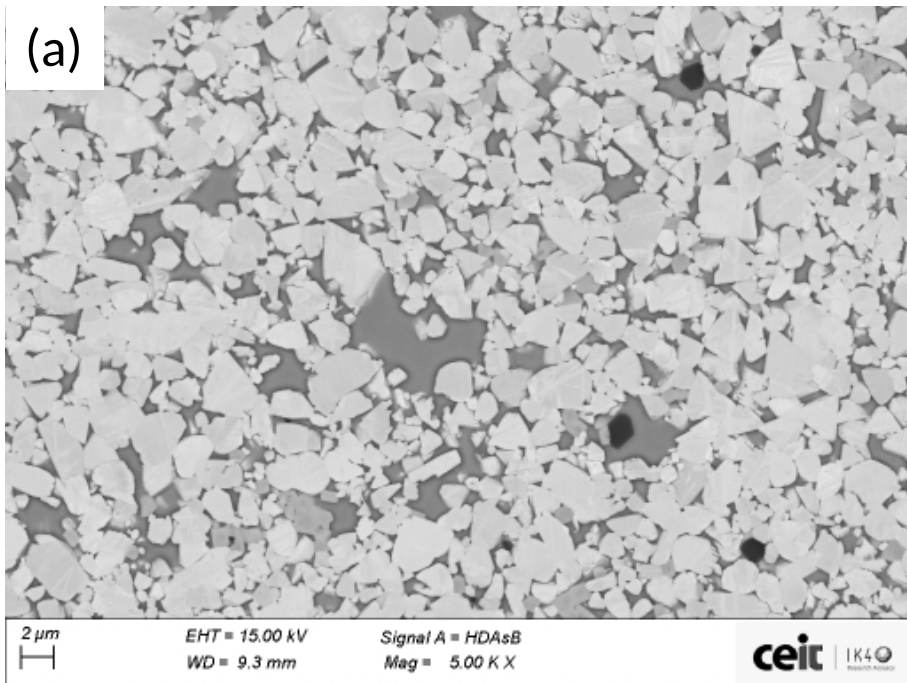






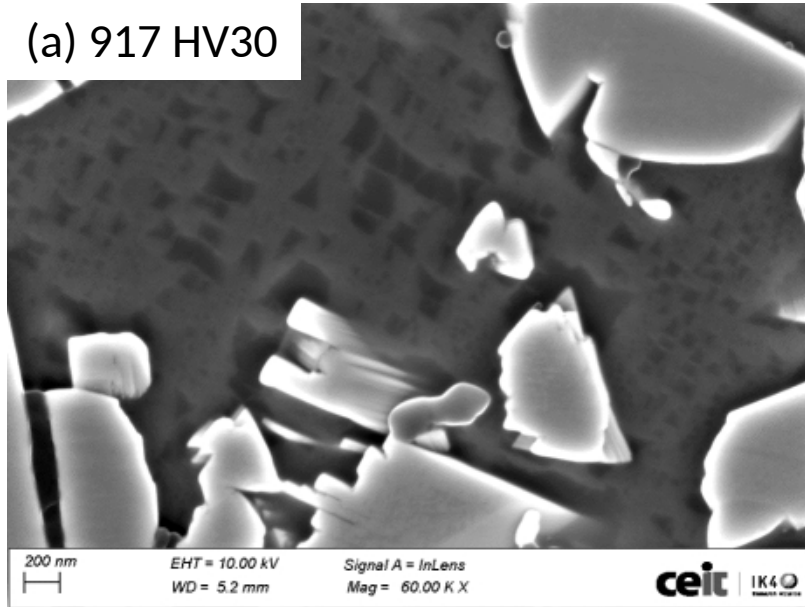




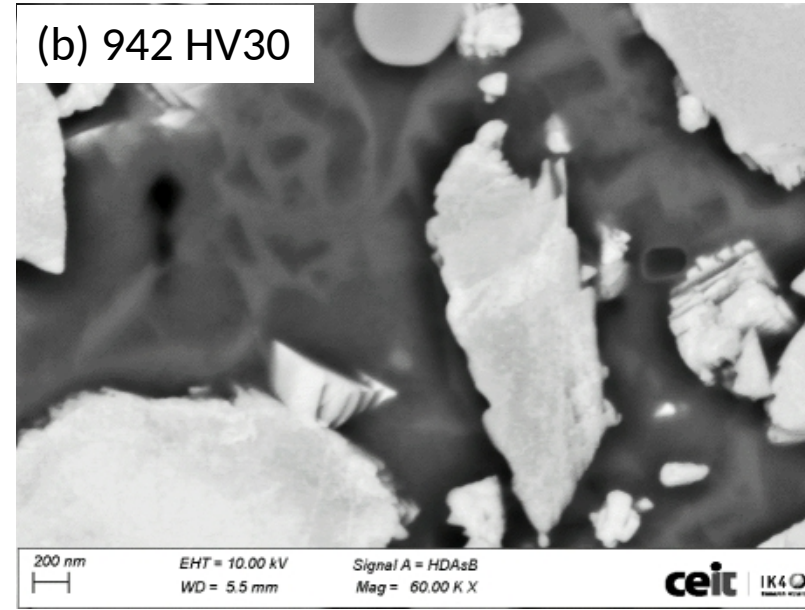




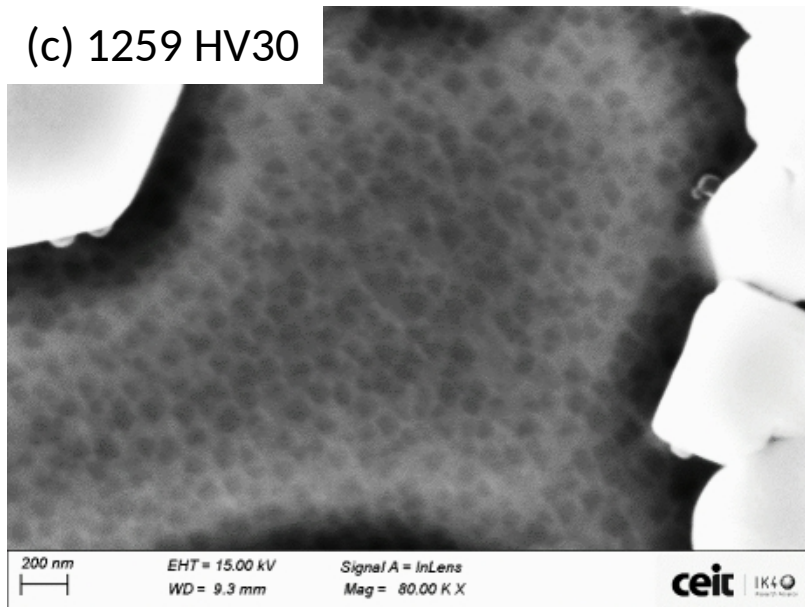
(a) 917 HV30



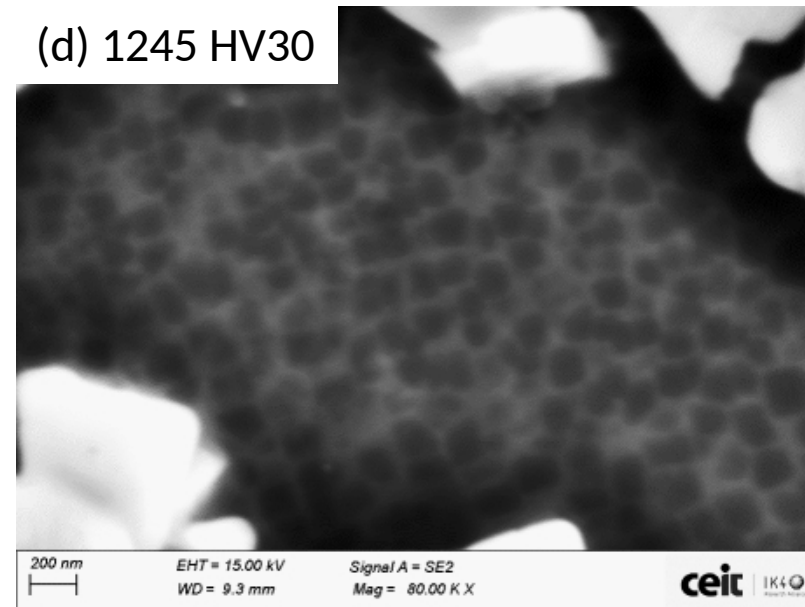
(b) 942 HV30



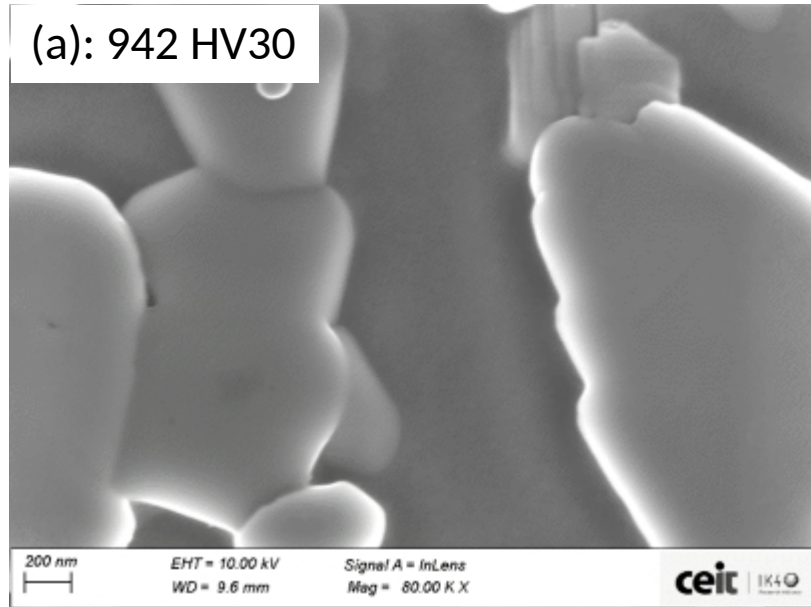
(c) 1259 HV30



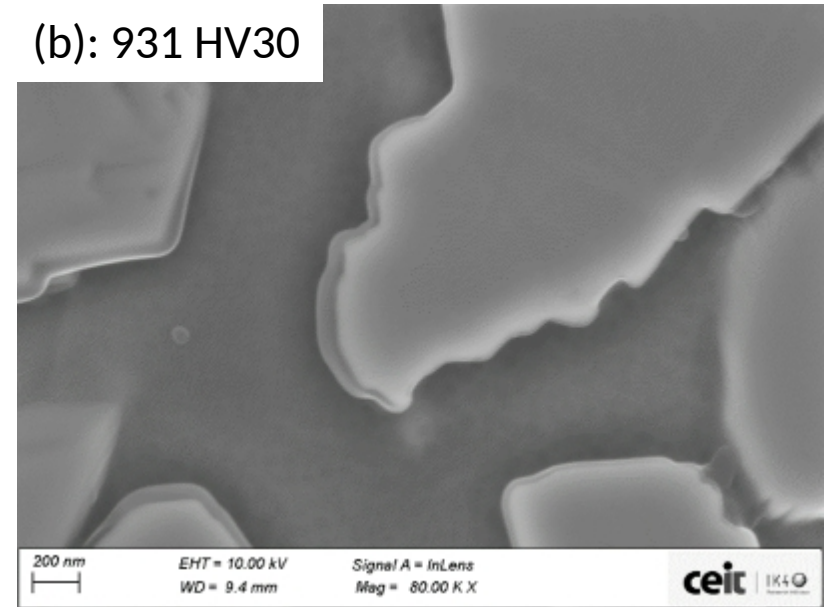
(d) 1245 HV30



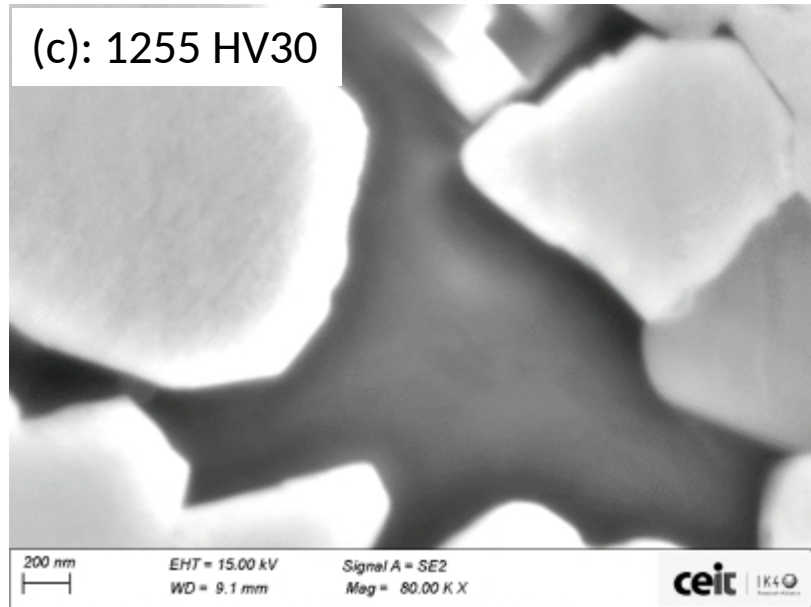
(a): 942 HV30



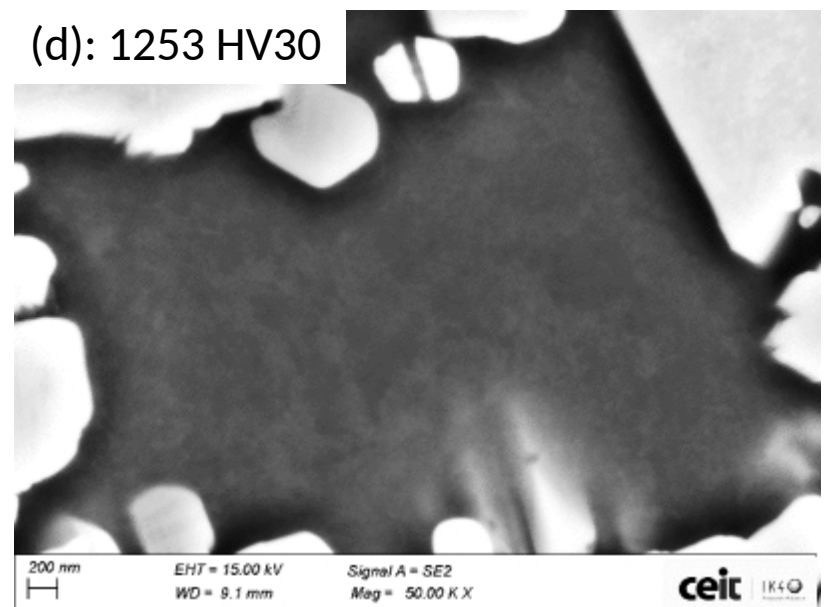
(b): 931 HV30



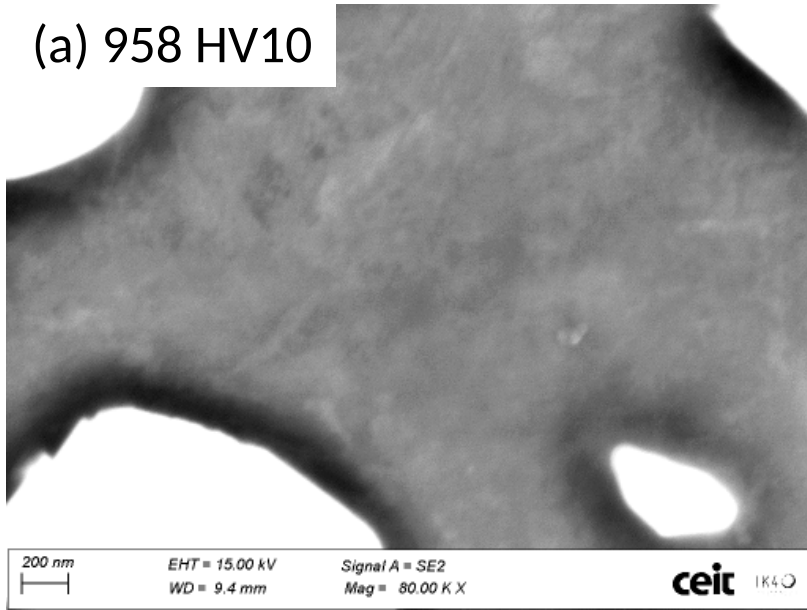
(c): 1255 HV30



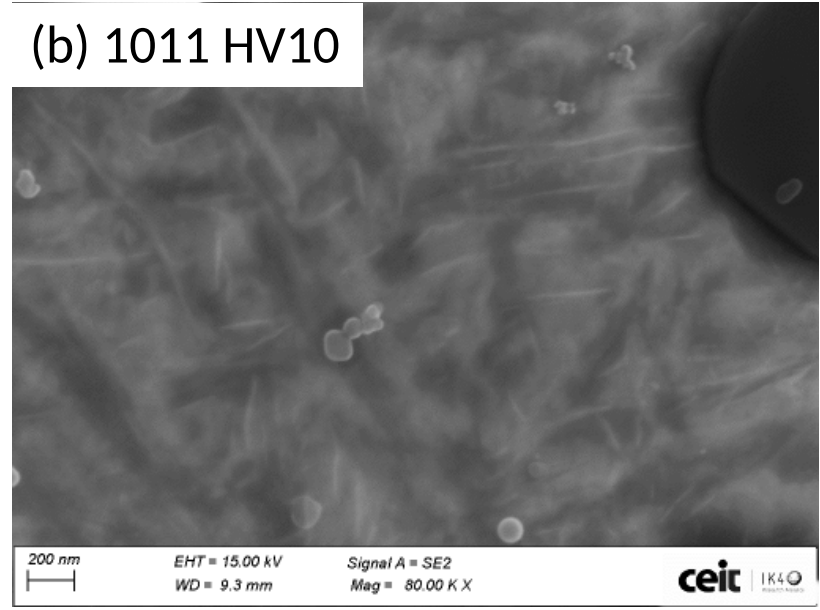
(d): 1253 HV30



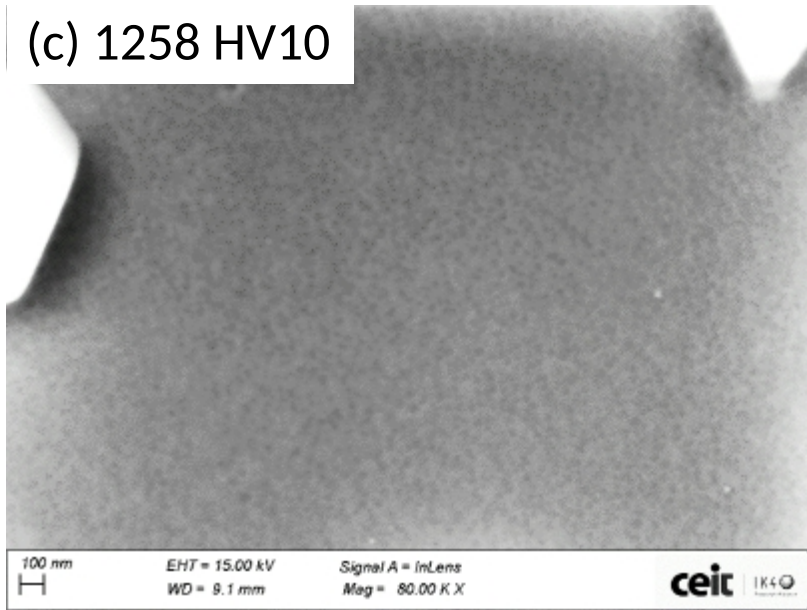
(a) 958 HV10



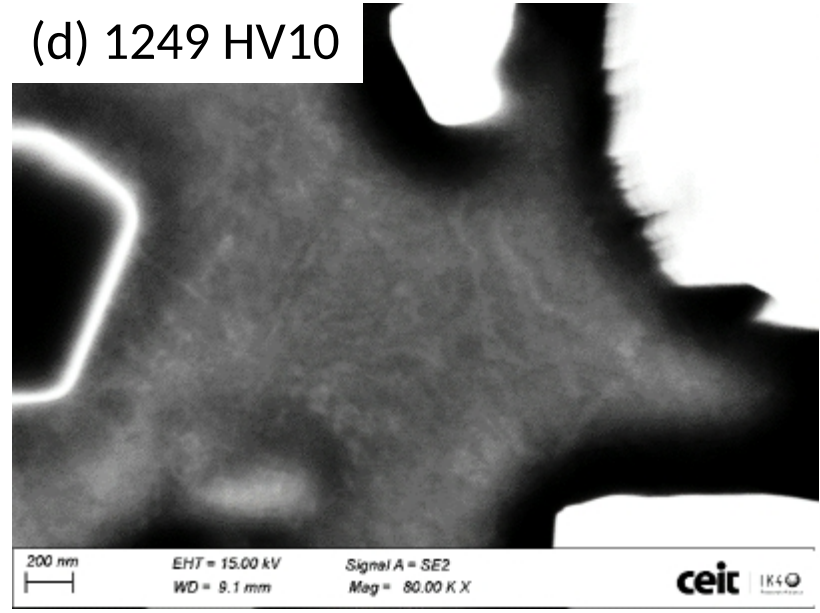
(b) 1011 HV10



(c) 1258 HV10



(d) 1249 HV10



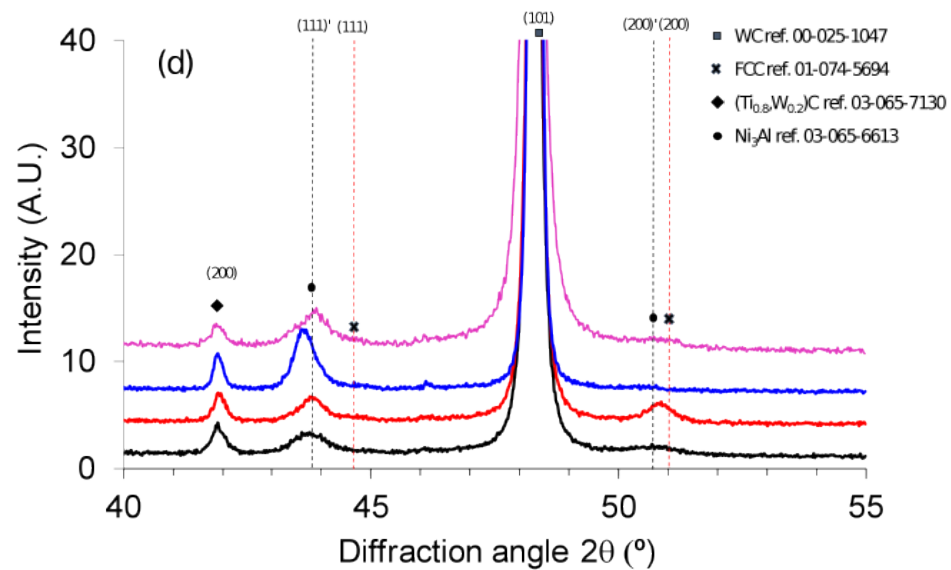
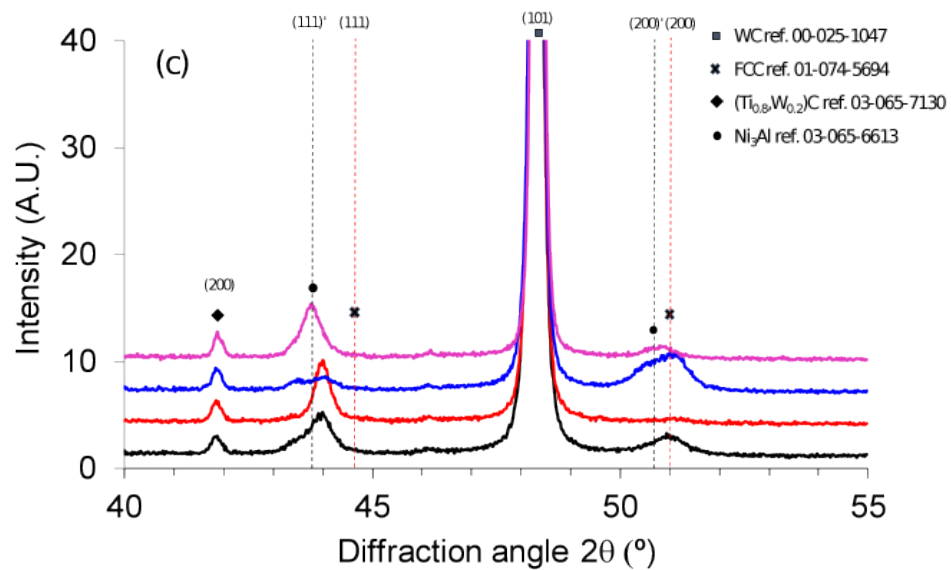
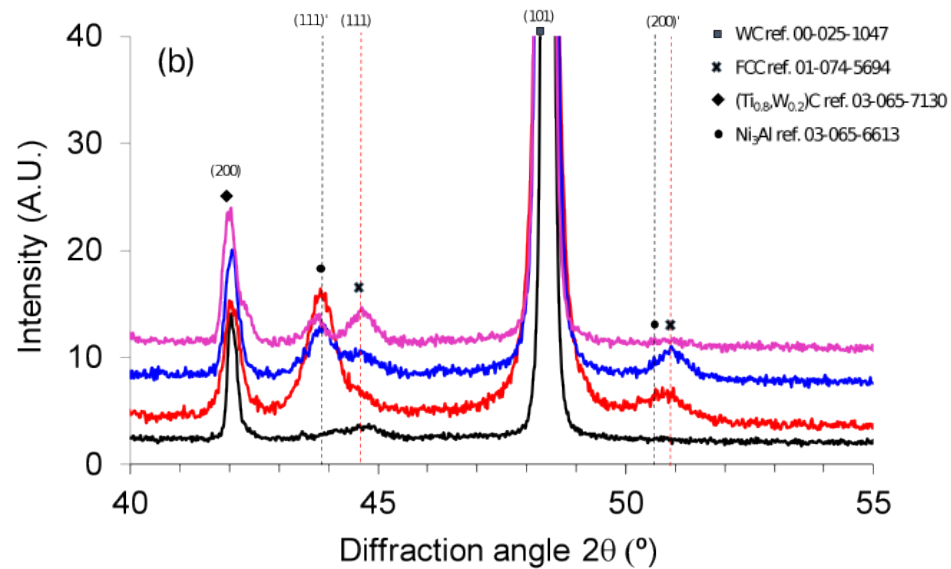
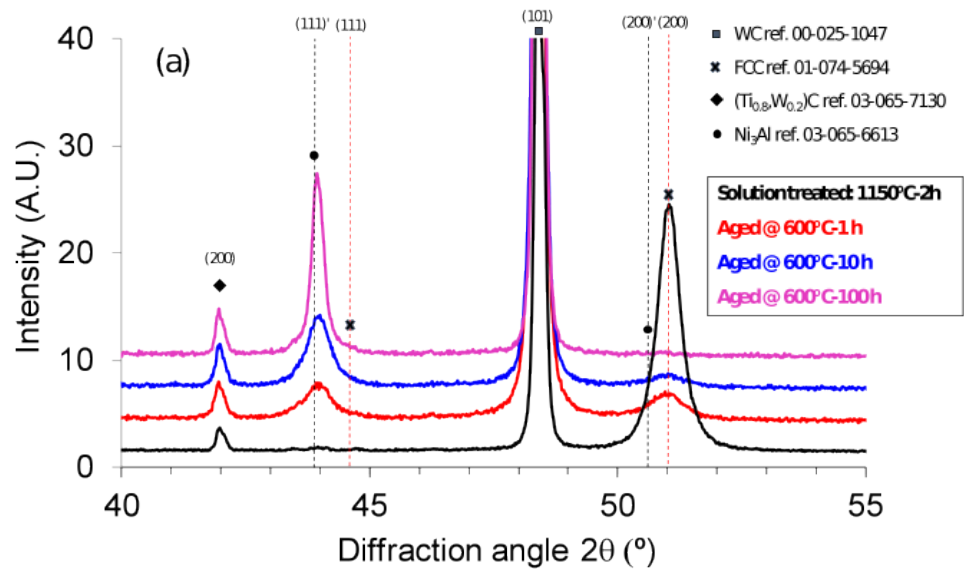


**Table 1.** Composition of the powder mixtures

<b>Ref.</b>	<b>WC</b>	<b>Co</b>	<b>Ni</b>	<b>Cr<sub>3</sub>C<sub>2</sub></b>	<b>TiAl<sub>3</sub></b>	<b>AlN</b>
<b>Alloy 1</b>	71.44	12.00	12.00	1.70	-	2.86
<b>Alloy 2</b>	71.30	12.00	12.00	1.70	3.00	-
<b>Alloy 3</b>	69.30	12.00	12.00	1.70	5.00	-
<b>Alloy 4</b>	85.65	6.00	6.00	0.85	1.5	-
<b>Alloy 5</b>	84.65	6.00	6.00	0.85	2.5	-

**Table 2.** Mean WC grain sizes and oxygen contents of Alloys 2 and 3 obtained after VS+HIP processing. Mean WC grain sizes were obtained by the mean linear intercept method. Oxygen contents were measured by IR spectrometry

	<b>Alloy 2</b>		<b>Alloy 3</b>	
<b>Mill rotation speed</b> (rpm)	100	200	100	200
<b>Mean WC grain size</b> ( $\mu\text{m}$ )	2.1	0.6	2.4	0.4
<b>Oxygen content</b> (wt.%)	0.15	0.33	0.32	0.50

**Table 3.** Effect of milling conditions on shrinkage rate and melting phenomena

Ref.	Milling rotation speed (rpm)	Temperature (°C)			
		Onset shrinkage rate peak	Shrinkage rate peaks	DSC melting onset	DSC melting peaks
Alloy 2	100	1248	1319 1338	1311	1362
	200	1250	1290 1322	1296	1342
Alloy 3	100	1302	1338	1310	1354
	200	1250	1328 1336	1285	1341
Alloy 4	100	1242	1281 1363	1286	1357
Alloy 5	100	1298	1305 1363	1304	1346

**Table 4.** Vickers hardness HV30 (ISO 3878) of WC-Co-Ni-Cr<sub>3</sub>C<sub>2</sub>-TiAl<sub>3</sub> materials for different heat treatment conditions

Composition	Vickers hardness HV30 (kg/mm <sup>2</sup> )				
	As HIPed	Solution treated	Aged @ 600°C-1 h	Aged @ 600°C-10 h	Aged @ 600°C-100 h
Alloy 2	917 ± 14	942 ± 11	942 ± 17	935 ± 13	958 ± 20
Alloy 3	942 ± 23	931 ± 8	931 ± 17	931 ± 6	1011 ± 17
Alloy 4	1259 ± 21	1255 ± 14	1248 ± 24	1265 ± 23	1258 ± 27
Alloy 5	1245 ± 31	1253 ± 12	1253 ± 25	1250 ± 6	1249 ± 17



## Declaration of interests

The authors declare that they have no known competing financial interests or personal relationships that could have appeared to influence the work reported in this paper.

The authors declare the following financial interests/personal relationships which may be considered as potential competing interests:

Corresponding autor on behalf of all coauthors

Jose M. Sanchez Moreno



**Tomas Soria:** Conceptualization, Data curation, Investigation. **Belen Lopez Ezquerra:** Data curation, Investigation. **Lorena Lozada:** Methodology **Jose M. Sanchez:** Supervision, Writing- Original draft preparation, Writing- Reviewing and Editing